








Thermal and Thermo-hydraulic Performance of Finned Double-Pass Solar Air Collector Utilizing Cylindrical Capsules Nano-Enhanced PCM

Jalal Assadeg^{1,2} , Kamaruzzaman Sopian¹ , Adnan Ibrahim^{1,‡} , Ahmad Fudholi¹ ,
Noshin Fatima³ , Ali H. A. Al-Waeli⁴ , Ag Sufiyan Abd Hamid^{5,†} 

¹ Solar Energy Research Institute, Universiti Kebangsaan Malaysia, 43600, Bangi, Selangor, Malaysia

² Renewable Energy Engineering Department, Faculty of Energy and Mining Engineering, Sebha University, P. O. Box 18758, Libya

³ Faculty of Engineering, Technology and Built Environment, UCSI University, Kuala Lumpur, 56000, Malaysia.

⁴ Engineering Department, American University of Iraq, Sulaimani, Kurdistan Region, Sulaimani, Iraq

⁵ Faculty of Science and Natural Resources, Universiti Malaysia Sabah, 88400 Kota Kinabalu, Sabah, Malaysia

(jassadeg@gmail.com, ksopian@ukm.edu.my, iadnan@ukm.edu.my, a.fudholi@ukm.edu.my, noshinfatima1990@gmail.com, ali9alwaeli@gmail.com, pian@ums.edu.my)

Corresponding Authors;

‡Adnan Ibrahim, Solar Energy Research Institute, Universiti Kebangsaan Malaysia, 43600, Bangi, Selangor, Malaysia, Tel: + 60 389118581, iadnan@ukm.edu.my

†Ag Sufiyan Abd Hamid, Faculty of Science and Natural Resources, Universiti Malaysia Sabah, 88400 Kota Kinabalu, Sabah, Malaysia, Tel; +6088 320000, pian@ums.edu.my

Received: 30.01.2023 Accepted: 23.02.2023

Abstract- Double-pass solar air collector with a finned absorber and nano-enhanced PCM in the lower channel is one of the significant and attractive designs proposed to improve the performance. This research paper presents a novel mathematical model of steady-state equilibrium equations created and developed for two air streams: the glass cover, absorber plate, fins, nano-enhanced PCM capsules, and back plate. The influence of various operating parameters on thermal and thermo-hydraulic performance was presented and discussed. The simulations were conducted at air mass flow rates from 0.02 kg/s through 0.06 kg/s and solar irradiance levels ranging from 475 W/m² to 1000 W/m². The proposed collector has an optimal energy efficiency of 80%, an exergy efficiency of 18.2% at solar irradiance of 1000 W/m² and a mass flow rate of 0.06 kg/s. The minimum and maximum improvement potentials for solar irradiance levels of 475–1000 W/m² at an ambient temperature of 298 K are 163–237 W. The proposed collector's best findings in the current study are 1.0 m in length and a width of roughly 0.3 m for air mass flow rates of 0.02-0.06 kg/s.

Keywords- Double-pass; DP-SAH; nanoparticles; Energy; Exergy; Paraffin wax.

Nomenclature

A_c	The collector's area (m ²)	Re	Reynolds number
A_{fin}	The fin's sectional area (m ²)	W_c	Width of the collector (m)
A_{Nano}	Surface area of nano-enhanced PCM capsules (m ²)	W_{fan}	Fan power (W)
CP_f	Constant pressure- specific heat of the air (J/kg. K).	V_{Nano}	Volume of nano- PCM capsules
C_v	Constant volume-specific heat of the air (J/kg. K).	T_{fo}	Outlet temperature of air (K)

$d1$	Depth of the upper air channel (m)	U_b	Back plate loss coefficient (W/m ² .K)
$d2$	Depth of the lower air channel(m)	U_t	Top loss coefficient (W/m ² .K)
D_h	Hydraulic diameter (m)	Greek Symbols	
h	Heat transfer coefficient (W/m ² .K)	α	Absorptivity
H_{fin}	Height of the fin (m)	ε	Emissivity
I_T	Incident solar irradiance on the collector (W/m ²)	τ	Transmittivity
IP	Improvement potential (W)	μ	Viscosity (N.s/m ²)
k_p	Thermal conductivity of absorber plate (W/m.K)	η	Efficiency (%)
L_c	Length of the collector (m)	ρ	Density (kg/m ³)
L_{fin}	Length of the fin (m)	σ	Stefan's Boltzmann constant (W/m ² .K ⁴)
L_{Nan}	Length of Nano-PCM capsule (m)	ϑ	Speed (m/s)
\dot{m}	Mass flow rate of operating fluid (kg/s)	ϑ_w	Wind speed (m/s)
CP_{Nan}	Constant pressure-specific heat of nano-PCM (J/kg. K).	ϑ_f	Air speed (m/s)
M_{ij}	Element used in Matrix	Subscripts	
n	Number of years	1 & 2	Upper and lower channel
N_{fin}	Number of the fins	a	ambient
N_{Nan}	Number of Nano-PCM capsules	b	back plate
Nu	Nusselt number	c	collector
Pr	Prandtl number	f	Fluid
Re	Reynolds number	fin	Fin
Q_{fin}	Heat transfer rate of fin (W)	g	Glass
Q_{pcm}	Heat transfer rate of Nano-PCM capsule (W)	i	Inlet
Q_u	Useful energy gain (W)	o	Outlet
T	Temperature (K)	p	absorber plate
T_{f1}	Temperature of air in upper duct (K)	s	Sun
T_{f2}	Temperature of air in lower duct (K)	th	thermo-hydraulic
T_p	Temperature of absorber (K)	W	wind
T_b	Temperature of black plate (K)		
T_{fi}	Inlet temperature of air (K)		

1. Introduction

Solar thermal collectors can create thermal energy by utilizing the incident of solar irradiance to heat working fluids. Many of these collectors are categorized based on the operating fluid (e.g., water or air-based), type of the fluid-carrying component (e.g., tubes, channels), and even their flow configurations (e.g., serpentine flow, double-pass flow). Also can be combined with other energy sources that are known as solar-assisted systems [1-5]. More research has utilized nanomaterials for heat transfer applications in the last decade, including solar collectors. Nanomaterials are nanosized particles with a diameter ranging from 1-100nm [6-10]. They exhibit high volume-to-surface ratios, and their size is minimal, allowing them to show high thermal conductivity. Moreover, the materials can be engineered to satisfy any desired properties to fit different applications by simply changing their compositions [11]. Nanofluids are used as working fluids for water-based solar collectors because of their excellent thermophysical properties. Nanofluids are mixtures of nanomaterials with base fluids. Another material used in the literature is phase change materials (PCM) [12]. These materials exhibit latent heat properties and can store and release large amounts of heat through the phase change cycle; however, PCM has poor thermal conductivity and thus might offer more resistance to heat flow in solar collectors [13-15].

Therefore, many researchers mix nanoparticles with PCM to enhance thermal conductivity. The mixtures are called "nano-PCM" [16-20]. Liu, et al. [21] reviewed the methods for improving the thermal characteristics of PCM and classified nanoparticle addition as "zero-dimensional" additives. These particles included metal and metal oxide nanoparticles as well. The researchers stated that using nanoparticles, which exhibit high thermal conductivity, with PCM is useful because, among other things, of their large specific surface area. [14], Sarafraz, et al. [22] used a cooling "jacket" or tank, for the thermal regulation of photovoltaic (PV) modules, by attaching it to the backside of the PV to enhance its electrical output and utilize the waste heat as thermal energy. The jacket was occupied with Multi-Wall Carbon Nanotubes (MWCNT)-Phase Change Materials (PCM).

The nano-PCM, along with nanofluids, operated within pipes to extract the heat from the jacket, aided in improving the collector's electrical and thermal power generation. The authors dispersed the nanoparticles within the PCM at 0.3 wt% to increase its thermal conductivity by 19%. Bondareva and Sheremet [23] numerically investigated using nano-enhanced pure n-octadecane poured within a closed copper radiator for improved thermal performance. The authors reported that the introduction of modest amounts of the nano-enhancers, Al₂O₃ nanoparticles, allowed for reducing the heat source's temperature and effectively enhanced the heat transfer within the PCM. The PCM can be integrated into thermal collectors

by (i) directly pouring them into a tank which is connected to the backplate, (ii) filling the collector's enclosure with PCM, (iii) To use PCM capsules, etc. The main challenge for solar thermal technology is to be economically viable and deliver higher thermal efficiencies for the end-user; thus, the researchers tried many modifications to improve and boost the thermal collector's heat transfer rate and its overall efficiency [24].

Omojaro & Aldabbagh investigated the performance of a finned single-pass and a double-pass solar air heater coupled with a steel wire mesh absorber. The finding indicates a considerable improvement in thermal efficiency when comparing the tested collectors with a conventional solar air heater [25]. The study focused on (i) the effects of combining a finned absorber plate and nano-enhanced PCM capsules into a double-pass solar air heater on outlet temperature and overall efficiency. (ii) the impact of solar irradiance levels [26, 27] and mass flow rates on the overall performance of the proposed collector, and (iii) varying the mass flow rates on the improvement potential and exergetic efficiency. Theoretically, five equations for the steady-state energy equilibrium were created and developed for the proposed collector. The most commonly utilized technique to address the energy balance equations in the mathematical model involves matrix inversion method, which is utilized to solve the equations. To model the proposed collector, the equations of energy balance were developed using MATLAB and then numerically simulated. The temperatures of the air collector components are assessed using a 5x5 matrix, which is iteratively solved through the "Matrix-inversion technique". The conditions included solar irradiance levels were varied from 475 to 1000 W/m², ambient temperature, and operational parameters such as the mass flow rates were varied from 0.02 to 0.06 kg/s. To simplify the analysis, some parameters were considered constant, such as the thermal conductivity across the fins and absorber. Assumed temperature values were utilized to assess different heat transfer coefficients and thermophysical properties. Matrixes [M], [T], and [C] were generated utilizing the assumed values and [M] was inverted to predict the mean temperatures of the collector's components.

2. Description of the System

Figures 1(a) and (b) illustrate two and three-dimensional drawings of the proposed collector. The glass cover, upper channel, absorber plate, lower channel, fins, nano-enhanced PCM capsules, back plate, and insulation are all shown in Figs. 1(a) and 1(b). The nano-PCM capsules absorb heat as air travels through the bottom air duct. As shown in the diagram, the air will enter the upper channel and move towards the lower channel before returning to the exit. Convection will absorb the heat from the finned absorber plate, and heat loss will be avoided by utilizing a glass cover and maintaining a tight fit. The heat from the absorber will be absorbed by the fins linked to the rear of the absorber plate via conduction, allowing more heat to flow into the air. Table 1 lists the materials used to construct the collector and its dimensions and specifications. The initial data was collected from the literature [28, 29] and then optimized as presented in Table 1.

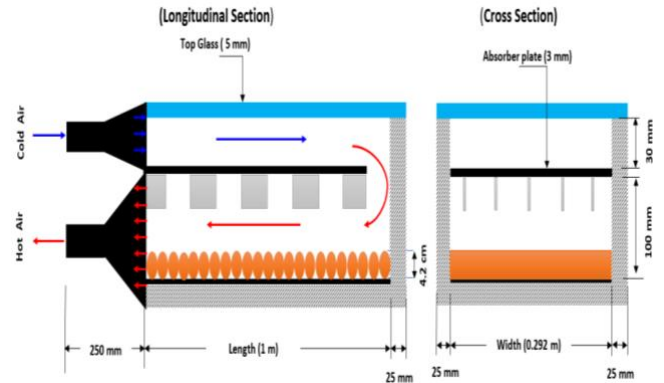


Fig. 1(a). Novel finned double-pass solar air collector with nano-enhanced PCM cylindrical capsules (2D drawing)

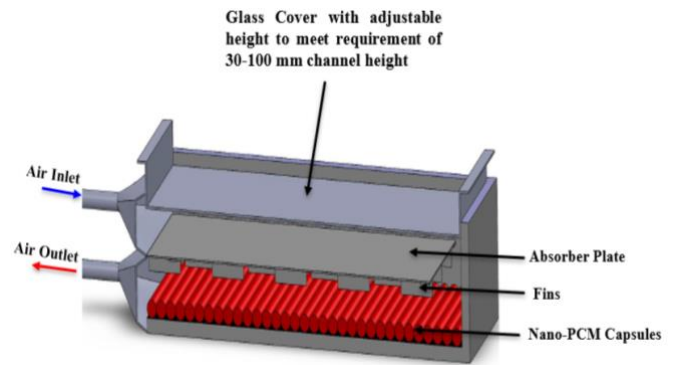


Fig. 1(b). Novel finned double-pass solar air collector with nano-enhanced PCM capsules (3D drawing).

2.1 Nano-Enhanced PCM Cylindrical Capsules

The nano-enhanced PCM capsule design and dimensions are illustrated in Fig. 2. The PCM used in the current study is Paraffin Wax which exhibits a high heat capacity; it absorbs and releases large quantities of energy sources during the charging and discharging process and at nearly constant temperatures [30]. Paraffin wax is a commonly used as phase change material due to its high heat capacity, relatively low cost, and compatibility with many construction materials. However, there are other PCMs available that may have advantages in certain applications [31-34]. One alternative PCM that has gained popularity in recent years is hydrated salts, such as calcium chloride hexahydrate and sodium sulfate decahydrate. These materials have a higher heat of fusion compared to paraffin wax, meaning they can store more energy per unit mass. However, they are typically more expensive and have a lower thermal conductivity than paraffin wax, which can result in slower charging and discharging times [32]. Another PCM option is fatty acids, such as stearic acid or palmitic acid. These materials have a higher melting point than paraffin wax, which can be advantageous in high-temperature applications. However, they have a lower heat of fusion and are more expensive than paraffin wax [35]. Overall, the paraffin wax allows for performance optimization by supplying thermal energy during cloudy times or at night and is useful for applications requiring thermal energy. The parameters of the tested paraffin wax are demonstrated in Table 2 [36].

Table 1. Specifications of proposed collector’s components

Component	Materials	Parameter	Value	Unit
Top glass	Glass	Thickness	5	mm
Upper air channel	-	Height	Adjustable	mm
		Length	1	m
		Width	0.292	m
Absorber plate	Aluminum	Thickness	3	mm
Lower air channel	-	Height	10	cm
		Length	1	m
		Width	0.3	m
Fins	Aluminum	Number	23	-
		Height	30	mm
		Length	10	cm
		Width	3	mm
Nano-PCM capsules	Stainless Steel	Number	23	-
		Length	29.2	cm
		Diameter	4.2	cm
		Thickness	2	mm
Backplate	Stainless Steel	Thickness	2	mm
Insulations	Rock wool	Thickness	2.5	cm

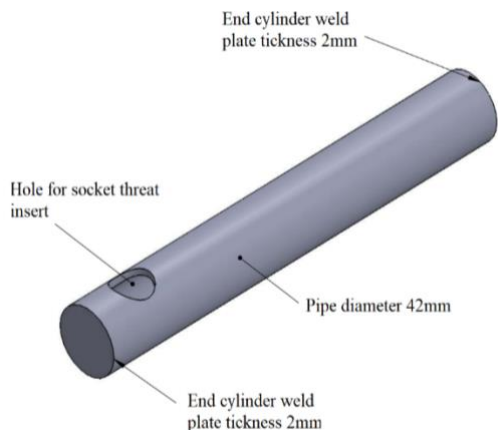


Fig. 2. The nano-enhanced PCM capsule of the collector

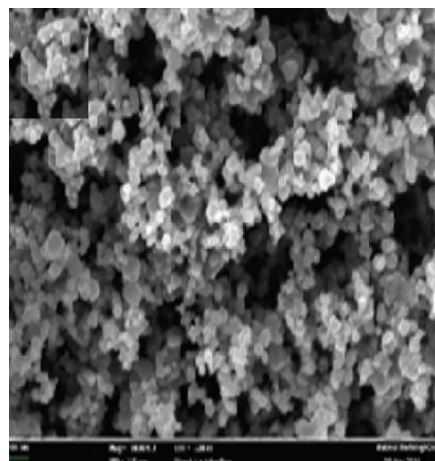


Fig. 3. SEM image of the Silicon Carbide (SiC)

Silicon carbide (SiC) was used as a nanoparticle in the studied collector. The incorporation of nanoparticles into the PCM led to an increase in its thermal conductivity [37]. Fig. 3 shows the Scanning Electron Microscopy (SEM) image taken for the nanoparticle of (SiC) and Table 3 shows the specification of the used nanoparticle (SiC).

Table 2. The thermophysical properties of (Paraffin wax)

Material Properties	Unit	Range
Melting point	°C	45
Latent heat	kJ/kg	195
Thermal conductivity	W/m.°C	0.21
Liquid state density	Kg/m ³	831
Liquid state-specific heat	kJ/kg.°C	2.1
Solid state density	Kg/m ³	930

Table 3. Specification of the used nanoparticle (SiC)

Item	Unit	Specification
Manufacturer	-	US Research Nanomaterial, Inc.
Appearance	-	Greyish white powder
PH value	-	3-7 at 20 °C
Grain size	nm	45-65 nm
Density	kg/m ³	3220
Thermal conductivity	W/m.K	370-490
Melting point	°C	2730
Molar point	g/mole	40.1
Zeta potential	mV	27.8
Loss on drying	% ≤	0.21

2.2 Staggered Rectangular Fins

The primary purpose of using fins is to enhance the area of heat transfer, which will ultimately result in an improvement in the heater's overall efficiency [38-40]. Because of this, the implications of fin height, number, and arrangement on performance were theoretically investigated using prepared mathematical model. Fig. 4 shows the design and configuration of the fins with its optimized nominals.

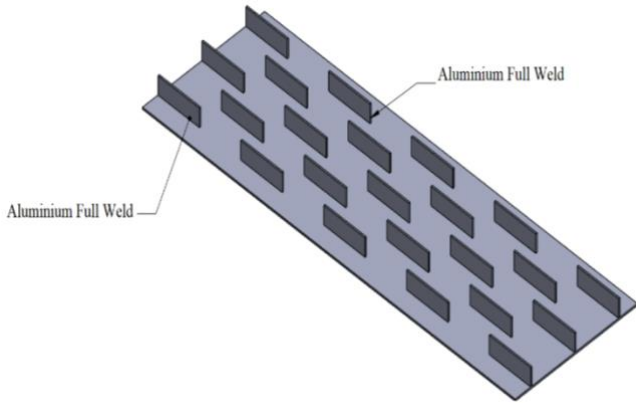


Fig. 4. Configuration of fins on the lower channel with height 30 mm and length 100 mm each.

3. Thermal Analysis

The proposed collector's steady-state balance equations are presented. The heat transfer coefficients, dimensions, and other parameters included in the mathematical model are shown in Fig. 5. Eq. (1) shows the mean air temperatures of the proposed solar collector:

$$T_f = (T_{fo} + T_{fi})/2 \tag{1}$$

Where the temperatures of inlet and outlet fluid are denoted using T_{fi} and T_{fo} , respectively.

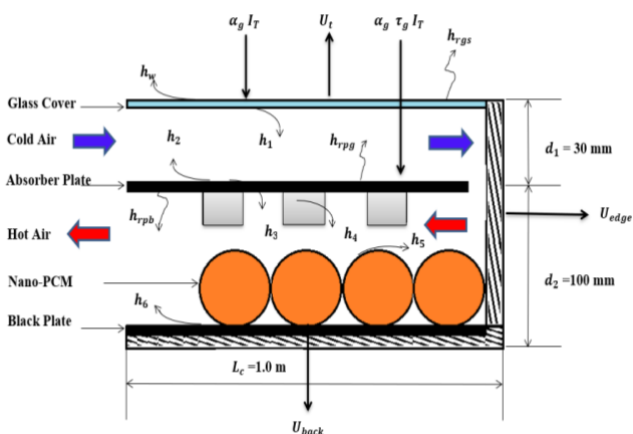


Fig.5. Schematic illustration of heat transfer coefficients for the proposed collector

The one-dimensional and steady-state balance equations of the glass cover, upper air channel, absorber plate, lower air channel, and back plate are as follows:

The thermal balance equation of the glass cover is written in Eq. (2).

$$U_t (T_g - T_a) + h_1 (T_g - T_{f1}) = h_{rpg} (T_p - T_g) + \alpha_g I_T \tag{2}$$

U_t, h, α and I_T represent the top loss coefficient, heat transfer coefficient, absorptivity, and solar irradiance respectively. While, small letters $g, a, f1$ and p denote glass, ambient, fluid first air channel and absorber plate, respectively

The upper air channel's thermal balance is shown in Eq. (3):

$$q_1 = h_1 (T_g - T_{f1}) + h_2 (T_p - T_{f1}) \tag{3}$$

Eq. (4) shows the thermal energy balance for the absorber plate:

$$\begin{aligned} h_{rpg} (T_p - T_g) + h_2 (T_p - T_{f1}) \\ + h_{rpb} (T_p - T_b) \\ + h_3 (T_p - T_{f2}) + \frac{N_{fin}}{A_c} Q_{fin} \\ = \alpha_g \tau_g I_T \end{aligned} \tag{4}$$

τ_g, N_{fin} and Q_{fin} represent the transmissivity of the glass cover, the number of fins and the heat transfer rate of the fin respectively. Eq. (5) shows the thermal energy balance for the lower air channel:

$$\begin{aligned} q_2 = h_3 (T_p - T_{f2}) + h_5 (T_b - T_{f2}) + \frac{N_{fin}}{A_c} Q_{fin} \\ + \frac{N_{Nano}}{A_c} Q_{Nano} \end{aligned} \tag{5}$$

The thermal energy balance for the backplate, as in Eq. (6), and the heat rates energy of the air along with the collector are shown in Eqs. (7) and (8):

$$\begin{aligned} h_{rpb} (T_p - T_b) = h_5 (T_b - T_{f2}) + U_b (T_b - T_a) \\ + \frac{N_{Nano}}{A_c} Q_{Nano} \end{aligned} \tag{6}$$

h_{rpb}, N_{Nano} and Q_{Nano} denote the radiative coefficient from absorber plate to back plate, the number of nano-PCM capsules and the heat transfer rate of the nano-PCM capsules respectively.

and

$$q_1 = 2 \dot{m} CP_f (T_{f1} - T_{fi}) / W_c L_c \tag{7}$$

$$q_2 = 2 \dot{m} CP_f (T_{f2} - 2T_{f1} + T_{fi}) / W_c L_c \tag{8}$$

CP_f, \dot{m}, W_c and L_c represent Constant pressure- specific heat of the air, mass flow rate of working fluid, Width of the collector and Length of the collector respectively.

Eq. (9) is used to determine the energy of convection heat transfer in nano-phase change materials [41-43] :

$$\begin{aligned} Q_{Nano} = \rho_{Nano} \times CP_{Nano} \\ \times V_{Nano} \frac{(T_{Nano} - T_{f2})}{\Delta t} \end{aligned} \tag{9}$$

$CP_{Nano}, \rho_{Nano}, V_{Nano}$ and T_{Nano} denote constant pressure-specific heat of nano-PCM, density of nano-PCM, volume of nano-PCM capsule and Temperature of nano-PCM capsule respectively. The calculation of the heat transfer through the conduction rate of fins, Eqs. (10) and (11) are used [29, 44]:

$$Q_{fin} = [2 h_4 k_p A_{fin} L_{fin}]^{1/2} (T_p - T_{f2}) \tanh KH_{fin} \tag{10}$$

$$K = \left(\frac{2 h_4 L_{fin}}{k_p A_{fin}} \right)^{1/2} \quad (11)$$

The Equations (2) to (11) above are represented in a pentagonal matrix from thermal balance equations as shown in Eq.(12):

$$[M_{ij}] [T_j] = [B_j] \quad (12)$$

In all the heat balance Eqs. (13) to (27), M_{ij} represent the temperature factors from M_{11} to M_{55} while C_j are constants C_1 to C_5 as follows:

$$C_1 = U_t T_a + \alpha_g I_T \quad (13)$$

$$C_2 = \left[\frac{-2 \dot{m} CP_f}{W_c L_c} \right] T_i \quad (14)$$

$$C_3 = \alpha_g \tau_g I_T \quad (15)$$

$$C_4 = -C_2 \quad (16)$$

$$C_5 = U_b T_a \quad (17)$$

$$M_{11} = h_1 + h_{rpg} + U_t \quad (18)$$

$$M_{22} = - \left[h_1 + h_2 + \left(\frac{2 \dot{m} CP_f}{W_c L_c} \right) \right] \quad (19)$$

$$M_{33} = h_2 + h_3 + h_{rpg} + h_{rpb} + \frac{N_{fin}}{A_c} [2 h_4 k_p A_{fin} L_{fin}]^{1/2} \tanh KH_{fin} \quad (20)$$

$$M_{34} = - \left[h_3 + \frac{N_{fin}}{A_c} [2 h_4 k_p A_{fin} L_{fin}]^{1/2} \tanh KH_{fin} \right] \quad (21)$$

$$M_{42} = \frac{4 \dot{m} CP_f}{W_c L_c} \quad (22)$$

$$M_{43} = -M_{34} \quad (23)$$

$$M_{44} = - \left[h_3 + h_5 + \frac{2 \dot{m} C_p}{W_c L_c} + \frac{N_{fin}}{A_c} [2 h_4 k_p A_{fin} L_{fin}]^{1/2} \tanh KH_{fin} \right] - \frac{N_{Nano}}{A_c} [\rho_{Nano} \times CP_{Nano} \times V_{Nano} \times 1/3600] \quad (24)$$

$$M_{45} = h_5 + \frac{N_{Nano}}{A_c} [\rho_{Nano} \times CP_{Nano} \times V_{Nano} \times 1/3600] \quad (25)$$

$$M_{54} = M_{45} \quad (26)$$

$$M_{55} = - \left[h_5 + h_{rpb} + U_b \right] - \frac{N_{Nano}}{A_c} [\rho_{Nano} \times CP_{Nano} \times V_{Nano} \times 1/3600] \quad (27)$$

$$\begin{bmatrix} M_{11} & -h_1 & -h_{rpg} & 0 & 0 \\ h_1 & M_{22} & h_2 & 0 & 0 \\ -h_{rpg} & -h_2 & M_{33} & M_{34} & -h_{rpb} \\ 0 & M_{42} & M_{43} & M_{44} & M_{45} \\ 0 & 0 & h_{rpb} & M_{54} & M_{55} \end{bmatrix} \begin{bmatrix} T_g \\ T_{f1} \\ T_p \\ T_{f2} \\ T_b \end{bmatrix} = \begin{bmatrix} C_1 \\ C_2 \\ C_3 \\ C_4 \\ C_5 \end{bmatrix} \quad (28)$$

Eq. (29) is employed to evaluate the useful energy gain and Eq. (30) is presented thermal efficiency of the proposed collector [45-47]:

$$Q_u = \dot{m}_f CP_f (T_{fo} - T_{fi}) \quad (29)$$

$$\eta_{en} = \frac{Q_u}{I_T \times A_c} \quad (30)$$

\dot{m}_f is mass air flow rate, CP_f is the specific heat of the air, A_c is of the collector area, which is equal to $W_c \times L_c$ and I_T stated as incident solar irradiance on the collector. The physical properties of operating fluid were assumed by Ong [29, 48-50]

The air-specific heat:

$$CP_f = 1005.7 + 0.000066 (T - 300) \quad (31)$$

The air density:

$$\rho_f = 1.1774 - 0.00359 (T - 300) \quad (32)$$

The air thermal conductivity:

$$k_f = 0.02624 + 0.0000758 (T - 300) \quad (33)$$

The air viscosity:

$$\mu_f = [1.983 + 0.00184(T - 300)] \times 10^{-5} \quad (34)$$

The heat transfer coefficients are calculated as in Equation 34 [49]:

$$h_w = 5.7 + 3.0 \vartheta_w$$

h_w is convection heat transfer coefficient due to wind and V_w (wind velocity). The radiative heat transfer coefficient between glass and sky as Eq. (36):

$$h_{rgs} = \frac{\sigma \varepsilon_g (T_g + T_{sky})(T_g^2 + T_{sky}^2)(T_g - T_{sky})}{T_g - T_a} \quad (36)$$

T_a is called ambient temperature and T_{sky} is known as sky temperature is calculated from the following formula in Eq. (37) [29, 48]:

$$T_{sky} = 0.0552 T_a^{1.5} \quad (37)$$

The radiative heat transfer coefficients (h_{rpg}), (h_{rppcm}) and (h_{rpb}) can be calculated from general formula between two parallel surfaces as shown in Eq. (38) :

$$h_{r12} = \frac{\sigma (T_2^2 + T_1^2) (T_2 + T_1)}{\frac{1}{\varepsilon_1} - \frac{1}{\varepsilon_2} - 1} \quad (38)$$

Eq. (39) is used to calculate the top loss coefficient U_t [49] :

$$U_t = \left(\frac{1}{h_w + h_{rgs}} \right) \quad (39)$$

The convective heat coefficients are calculated by using Equation 39:

$$h_{1,2,3,4,5,6} = \frac{k}{D_h} Nu \quad (40)$$

The Nusselt Number for the laminar flow region ($Re < 2300$) [48, 51] :

$$N_{u} = 5.4 + \frac{0.00190 \left[Re Pr \left(\frac{D_h}{L_c} \right) \right]^{1.71}}{1 + 0.00563 \left[Re Pr \left(\frac{D_h}{L_c} \right) \right]^{1.17}} \quad (41)$$

The Nusselt Number for the transition flow region (2300 Re < 6000) [48, 51]:

$$N_{u} = 0.116 \left(R_e^{\frac{2}{3}} - 125 \right) Pr^{\frac{1}{3}} \left[1 + \left(\frac{D_h}{L_c} \right)^{2/3} \right] \left(\frac{\mu}{\mu_w} \right)^{0.14} \quad (42)$$

The Nusselt Number for the turbulent flow region ($Re > 6000$) [48, 51]:

$$N_{u} = 0.018 R_e^{0.8} Pr^{0.4} \quad (43)$$

D_h is the hydraulic diameter of the ducts and Pr is Prandtl's Number of working fluids and Re is the Reynolds number calculated from the following equations [29, 51]

$$Re = \frac{\vartheta_f \rho_f D_h}{\mu_f} \quad (44)$$

$$\vartheta_f = \frac{\dot{m}_f}{\rho_f W_c d} \quad (45)$$

$$D_h = \frac{4 W_c d}{2 (W_c + d)} \quad (46)$$

4. Thermo-hydraulic Analysis

The efficiency of thermo-hydraulic (η_{th}) of the proposed collector [52, 53]:

$$\eta_{th} = \frac{(Q_u - W_{fan})}{I_T \times A_c} \quad (47)$$

Q_u is useful energy gain and W_{fan} (the amount of fan power necessary to force the operating fluid throughout the collector). The fan power is calculated as:

$$W_{fan} = \frac{P_p}{\eta_{fan} \times \eta_{motor}} \quad (48)$$

η_{fan} (Efficiency of fan) and η_{motor} (efficiency of motor) = 0.9 and the pumping power can be defined:

$$P_p = \frac{\dot{m}_f \Delta P}{\rho_f} \quad (49)$$

$$\Delta P = \left(\frac{\dot{m}_f}{A_{ap}} \right)^2 \frac{1}{\rho_f} \left(\frac{L_c}{D_h} \right)^3 f \quad (50)$$

A_{ap} is the air passage area of the air ($L_c \times d$) and f (friction factor for Reynolds numbers) are determined from equations [54-56]:

For $Re < 2550$

$$f = \frac{24}{Re} + 0.9 \left(\frac{d}{L_c} \right) \quad (51)$$

For $2550 < Re < 10^4$

$$f = 0.0094 + 2.92 Re^{-0.15} \left(\frac{d}{L_c} \right) \quad (52)$$

For $10^4 < Re < 10^5$

$$f = 0.059 Re^{-0.2} + 0.73 \left(\frac{d}{L_c} \right) \quad (53)$$

The total pressure drops (ΔP) for the double-pass solar air collector can be calculated using Eq. (53):

$$\Delta P = \Delta P_{ch1} + \Delta P_{ch2} \quad (54)$$

The exergy efficiency (η_{ex}) and improvement potential and (IP) of the proposed collector can be obtained from Eqs. (55) and (56) based on Gool [57]:

$$\eta_{ex} = 1 - \frac{\dot{E}x_d}{\dot{E}x_i} \quad (55)$$

$$IP = (1 - \eta_{ex}) \dot{E}x_d \quad (56)$$

Where $\dot{E}x_i$ is Exergy input of solar irradiance and $\dot{E}x_d$ is Exergy destruction.

5. Results and Observations

The performance of the proposed collector is assessed utilizing various mass flow rates and solar irradiance values. The collector's thermal and hydraulic efficiency has been evaluated, as shown in Fig. 6. The thermal efficiency is just 0.9% more than the hydraulic efficiency. Since the hydraulic efficiency accounts for the power loss in the fan, it will always be lower than the thermal efficiency. The lower the hydraulic efficiency, the more power is required for a fan to move a mass of air at a certain pace.

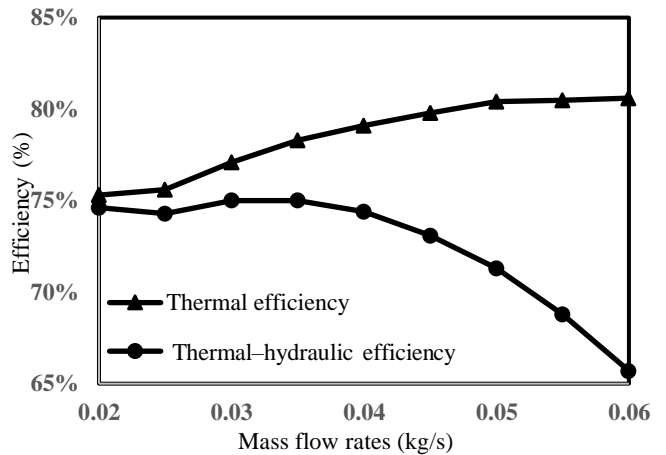


Fig. 6. Thermal and Thermal-hydraulic efficiencies of the proposed collector versus air mass flow rates for $I_T=1000W/m^2$

Most of the research focuses solely on achieving the highest possible thermal efficiency without accounting for power losses caused by fans, blowers, and pumps. When power losses are considered, an air mass flow of 0.03kg/s produces the greatest results, with a 75% efficiency. If solar irradiation and mass flowrate efficiency are the primary considerations, running the collector at 0.06kg/s results in maximum thermal efficiency of 80%. At 0.06 kg/s, the thermal efficiency is approximately 22.3% more than the thermal-hydraulic efficiency. At a total solar irradiation of 1000W/m², Fig. 7 shows both outlet temperature and exergy efficiency versus different air flow rates from 0.02 through 0.06 kg/s. With the addition of the mass flow rate of air, the temperature of the output air will decrease. The air moves faster via the channels, allowing for a shorter heating time. However, because more of it goes through, the temperature decline in the output air is neither linear nor continuous. The temperature drops more quickly initially, between 0.02kg/s and 0.03kg/s, a loss of 1.16%. When the mass flow rate rises to 0.04 kg/s, the temperature drops by 0.59%, and at 0.05 kg/s, the temperature

drops by 0.36%. The highest exergy efficiency is recorded at 0.02kg/s; then, as the air mass flow rate increases, the efficiency decreases, which is also due to energy losses. Unlike thermal efficiency, the peak exergy efficiency is only 22.7%. It is noteworthy that thermal energy is low-grade energy because heat rapidly dissipates.

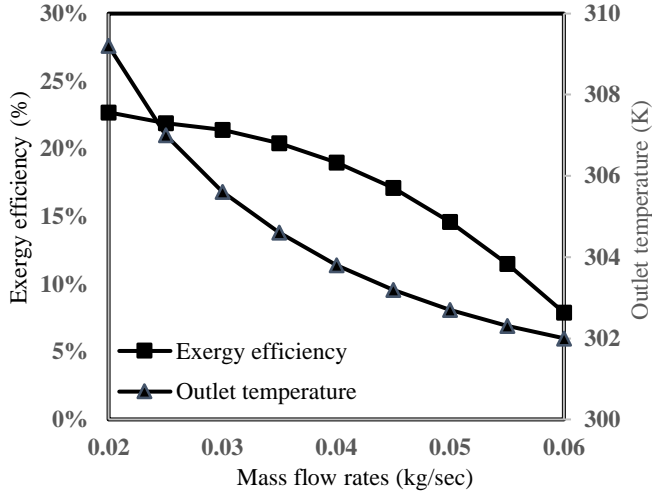


Fig. 7. The efficiency of exergy and temperature at the proposed collector outlet versus air mass flow rates of $I_T=1000W/m^2$

The lowest exergy efficiency is 7.9% at the mass flux is 0.06 kg/s. The drop-in exergy efficiency increases with the increase in mass flow rate, as it begins with a drop of 5.7% when varying the mass flow rate from 0.02kg/s to 0.03 kg/s. Then increasing the mass flow rate to 0.04 kg/s leads to a drop in exergy efficiency of 11.2%. At 0.05 kg/s, the exergetic efficiency decreases by 23.1%. Finally, when increasing mass flux from 0.05 to 0.06 kg/s, exergetic efficiency drops by 45.8%. This is also because heat is low-grade energy, and the increased mass flow rate requires increased fan power. Fig. 8 showcases the extent to which the fan power increases with respect to how much useful heat the collector produces at an incident solar irradiance of 1000 W/m². Minimal change is observed in useful heat gain with the increments in mass flow rate, where the heat produced is 225.9 W at 0.02 kg/s, and it reaches 231.5 W at 0.03 kg/s a 2.47% increase. At 0.04 kg/s, the increase reaches 2.59%. The increase in heat production will continue to drop in its amount as the mass flow rate increases until it stabilizes at a certain range. Nonetheless, the drop in the increased production of the thermal-hydraulic and exergetic efficiencies showcases that improving the thermal performance by simply increasing the mass flow rate is not a viable solution.

The exergetic efficiency of the studied collector is only maximized if the exergy losses are minimized. Therefore, the concept of Improvement Potential (IP) is used to analyze this process of solar air heating. Fig. 8 shows the improvement potential of the proposed collector as the mass flow rate is varied from 0.02 to 0.06 kg/s and for incident solar irradiance values of 475, 675, 875, and 1000 W/m². The highest IP is around 237.4 W, which occurs if the collector receives 1000 W/m² of solar irradiance. The graph depicts how increased

sun irradiance increases improvement potential by allowing more energy into the system, as shown in Fig. 9.

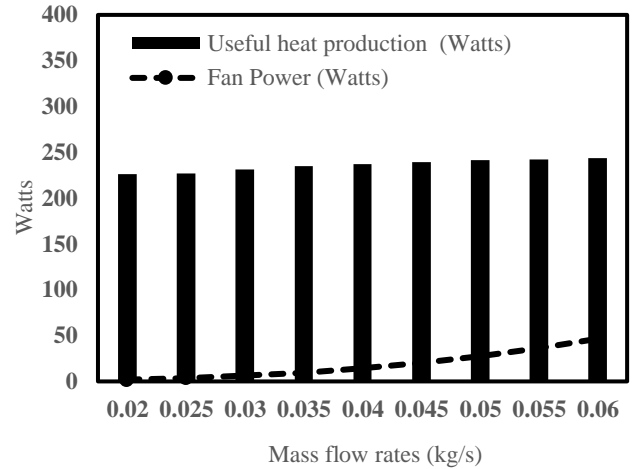


Fig. 8. Useful heat gain and power of fan of the studied collector versus air mass flow rates of $I_T=1000W/m^2$.

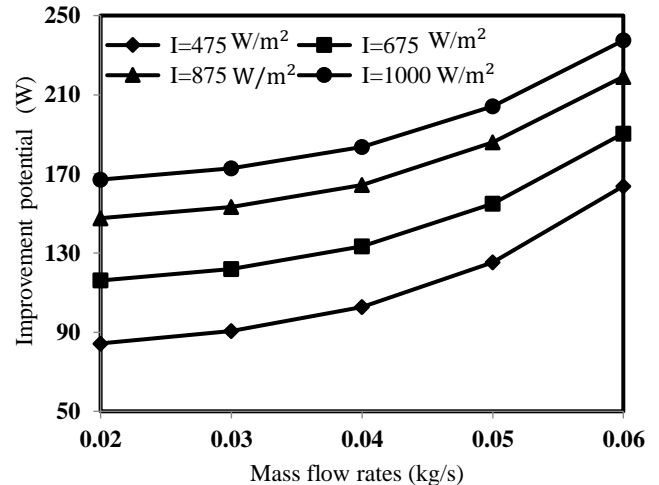


Fig. 9. The proposed collector's improvement potential versus mass flow rates at different solar irradiance levels

6. Conclusion

This research paper presented a numerical analysis of a proposed collector's performance by developing a steady-state energy balance model to represent the collector design and account for the collector's components. The main features of this collector are the use of rectangular longitudinal fins in a zigzag pattern and the nano-phase change materials (nano-PCM) stored within capsules. Different mass flow rates, ranging from 0.02 to 0.06kg/s, were used to view the changes in the collector's performance. The thermal, thermo-hydraulic, and exergy efficiencies were analyzed, as were the outlet air-fluid temperature and improvement potential. The following are the study's main findings:

- Increasing the mass flux of air from 0.02 to 0.06 kg/s led to an increase in the thermal efficiency of the proposed collector from 75.3 to 80%, respectively, at an incident solar irradiance level of 1000 W/m².

- When the mass flux increases from 0.02 to 0.06 kg/s, the thermo-hydraulic efficiency falls from 74.6 to 65.7%.
- The peak thermal efficiency is 80%, achieved when the studied collector is subjected to 1000W/m² and operates at a mass flow rate of 0.06 kg/s. While peak thermo-hydraulic efficiency is 75%, which is achieved for the same solar irradiance (1000 W/m²) but at a mass flow rate of 0.03 kg/s
- The outlet air temperature drops with the increase in the mass flow rate. The temperature peaks at 309.2 K when the mass flow rate is 0.02 kg/s, and it reaches its lowest point, which is 302 K when mass flux of the air is 0.06 kg/s.
- The peak exergetic efficiency is 22.7% when the mass flow rate, solar irradiance, and ambient temperature are around 0.02 kg/s, 1000 W/m² and 298.16 K. The improvement potential is at its highest, around 237.4 W, when the solar irradiance is 1000 W/m² at the mass flux of the air is 0.06 kg/s.

In addition, for further improvement some parameters such as air humidity effect on the collector was neglected in this study. So, if it would be considered in future work, the results will be more reliable and similar to the real physical processes in the system.

Acknowledgement

The authors would like to acknowledge the Ministry of Higher Education of Malaysia under the Fundamental Research Grant Scheme (FRGS/1/2019/TK07/UKM/02/4) and the Faculty of Science and Natural Resources, Universiti Malaysia Sabah (UMS) under SPBK-UMS phase 1/2022 (SBK0518-2022) (UMS) research grants.

References

- [1] L. Evangelisti, R. De Lieto Vollaro, and F. Asdrubali, "Latest advances on solar thermal collectors: A comprehensive review," *Renewable and Sustainable Energy Reviews*, vol. 114, p. 109318, 2019/10/01/ 2019.
- [2] V. Msomi and O. Nemraoui, "Improvement of the performance of solar water heater based on nanotechnology," in *2017 IEEE 6th International Conference on Renewable Energy Research and Applications (ICRERA)*, 2017: IEEE, pp. 524-527.
- [3] R. Shirin, A. S. Abd Hamid, K. Sopian, H. Jarimi, A. Bassim, and A. Ibrahim. "Heat Transfer Analysis of the Flat Plate Solar Thermal Collectors with Elliptical and Circular Serpentine Tubes" *Applied Sciences* 12, no. 9: 4519. <https://doi.org/10.3390/app12094519>, 2022
- [4] F. Ghasemzadeh, "Advanced Study of the Parabolic Trough Collector Using Aluminum (III) Oxide Seal," *International Journal of Smart Grid-ijSmartGrid*, vol. 4, no. 3, pp. 111-116, 2020.
- [5] S. H. Zanjani, H. Shahinzadeh, A. B. Oskui, W. Yaïci, M. Longo, and S. M. Zanjani, "Performance Assessment of Heat Pump and Solar Thermal Heating with Seasonal Storage Systems for Smart Microgrid Research Center Building at IAUN," in *2022 10th International Conference on Smart Grid (icSmartGrid)*, 2022: IEEE, pp. 345-350.
- [6] D. K. Devendiran and V. A. Amirtham, "A review on preparation, characterization, properties and applications of nanofluids," *Renewable and Sustainable Energy Reviews*, vol. 60, pp. 21-40, 2016/07/01/ 2016.
- [7] S.-B. Chen, S. Saleem, M. N. Alghamdi, K. S. Nisar, A. Arsalanloo, A. Issakhov, and W.-F. Xia, "Combined effect of using porous media and nano-particle on melting performance of PCM filled enclosure with triangular double fins," *Case Studies in Thermal Engineering*, vol. 25, p. 100939, 2021/06/01/ 2021.
- [8] R. Elarem, T. Alqahtani, S. Mellouli, W. Aich, N. Ben Khedher, L. Kolsi, and A. Jemni, "Numerical study of an Evacuated Tube Solar Collector incorporating a Nano-PCM as a latent heat storage system," *Case Studies in Thermal Engineering*, vol. 24, p. 100859, 2021/04/01/ 2021.
- [9] L. Liu, J. Li, J. Niu, and J.-Y. Wu, "Evaluation of the energy storage performance of PCM nano-emulsion in a small tubular heat exchanger," *Case Studies in Thermal Engineering*, vol. 26, p. 101156, 2021/08/01/ 2021.
- [10] H. Hussein, "The state of the art of nanomaterials and its applications in energy saving," *Bulletin of the National Research Centre*, vol. 47, no. 1, pp. 1-22, 2023.
- [11] D. Golberg, P. M. Costa, M. S. Wang, X. Wei, D. M. Tang, Z. Xu, Y. Huang, U. K. Gautam, B. Liu, and H. Zeng, "Nanomaterial engineering and property studies in a transmission electron microscope," *Advanced materials*, vol. 24, no. 2, pp. 177-194, 2012.
- [12] T. Bouhal, T. El Rhafiki, T. Kousksou, A. Jamil, and Y. Zeraouli, "PCM addition inside solar water heaters: Numerical comparative approach," *Journal of Energy Storage*, vol. 19, pp. 232-246, 2018.
- [13] F. Frusteri, V. Leonardi, S. Vasta, and G. Restuccia, "Thermal conductivity measurement of a PCM based storage system containing carbon fibers," *Applied thermal engineering*, vol. 25, no. 11-12, pp. 1623-1633, 2005.
- [14] S. Kyaligonza and E. Cetkin, "Photovoltaic System Efficiency Enhancement with Thermal Management: Phase Changing Materials (PCM) with High Conductivity Inserts," *International Journal of Smart Grid-ijSmartGrid*, vol. 5, no. 4, pp. 138-148, 2021.
- [15] I. Amar Fahmi, A. S. Abd Hamid, A. Ibrahim, H. Jarimi, and K. Sopian. "Performance Analysis of a Double Pass Solar Air Thermal Collector with Porous Media Using Lava Rock" *Energies* 15, no. 3: 905. <https://doi.org/10.3390/en15030905>, 2022
- [16] M. Al-Jethelah, S. H. Tasnim, S. Mahmud, and A. Dutta, "Nano-PCM filled energy storage system for solar-thermal applications," *Renewable Energy*, vol. 126, pp. 137-155, 2018/10/01/ 2018.

- [17] S. Rostami, M. Afrand, A. Shahsavari, M. Sheikholeslami, R. Kalbasi, S. Aghakhani, M. S. Shadloo, and H. F. Oztop, "A review of melting and freezing processes of PCM/nano-PCM and their application in energy storage," *Energy*, vol. 211, p. 118698, 2020.
- [18] S. Ebadi, S. H. Tasnim, A. A. Aliabadi, and S. Mahmud, "Melting of nano-PCM inside a cylindrical thermal energy storage system: Numerical study with experimental verification," *Energy Conversion and Management*, vol. 166, pp. 241-259, 2018.
- [19] A. Sathishkumar and M. Cheralathan, "Charging and discharging processes of low capacity nano-PCM based cool thermal energy storage system: An experimental study," *Energy*, vol. 263, p. 125700, 2023.
- [20] A. M. Bassam, K. Sopian, A. Ibrahim, M. F. Fauzan, A. B. Al-Aasam, and G. Y. Abusaibaa, "Experimental analysis for the photovoltaic thermal collector (PVT) with nano PCM and micro-fins tube nanofluid," *Case Studies in Thermal Engineering*, vol. 41, p. 102579, 2023.
- [21] W. Liu, X. Zhang, J. Ji, Y. Wu, and L. Liu, "A Review on Thermal Properties Improvement of Phase Change Materials and its Combination with Solar Thermal Energy Storage," *Energy Technology*, 2021.
- [22] M. Sarafraz, M. R. Safaei, A. S. Leon, I. Tlili, T. A. Alkanhal, Z. Tian, M. Goodarzi, and M. Arjomandi, "Experimental investigation on thermal performance of a PV/T-PCM (photovoltaic/thermal) system cooling with a PCM and nanofluid," *Energies*, vol. 12, no. 13, p. 2572, 2019.
- [23] N. S. Bondareva and M. A. Sheremet, "Effect of nano-sized heat transfer enhancers on PCM-based heat sink performance at various heat loads," *Nanomaterials*, vol. 10, no. 1, p. 17, 2020.
- [24] T. Alam and M.-H. Kim, "Performance improvement of double-pass solar air heater—A state of art of review," *Renewable and Sustainable Energy Reviews*, vol. 79, pp. 779-793, 2017.
- [25] A. Omojaro and L. Aldabbagh, "Experimental performance of single and double pass solar air heater with fins and steel wire mesh as absorber," *Applied energy*, vol. 87, no. 12, pp. 3759-3765, 2010.
- [26] M. Alghoul, J. ASSADEQ, M. SULAIMAN, H. KHAMIES, M. YAHYA, E. M. ALFEGI, A. ZAHARIM, and K. SOPIAN, "Evaluation of Water Vapour Thickness on Solar Radiation Budget," 2009.
- [27] M. Alghoul, H. Khamies, M. Sulaiman, J. Assadeq, M. Yahya, M. Alfegi, A. Zaharim, and K. Sopian, "Impact of aerosol optical depth on solar radiation budget," in *Proc. 3rd WSEAS Int. Conf. Energy Planning, Energy Saving, Environ. Educ. EPESE*, 2009, vol. 9, pp. 386-393.
- [28] A. Fudholi, M. Zohri, G. L. Jin, A. Ibrahim, C. H. Yen, M. Y. Othman, M. H. Ruslan, and K. Sopian, "Energy and exergy analyses of photovoltaic thermal collector with ∇ -groove," *Solar Energy*, vol. 159, pp. 742-750, 2018/01/01/ 2018.
- [29] A. Fudholi, K. Sopian, M. Y. Othman, M. H. Ruslan, and B. Bakhtyar, "Energy analysis and improvement potential of finned double-pass solar collector," *Energy Conversion and Management*, vol. 75, pp. 234-240, 2013/11/01/ 2013.
- [30] O. Abou Saima and A. A. Abdel-Rehim, "Experimental and numerical analysis for the size, charging and discharging characteristics of a phase changing material as a thermal energy storage," *Journal of Energy Storage*, vol. 58, p. 106228, 2023/02/01/ 2023.
- [31] R. Ye, H. Jiang, J. Wang, X. Yang, and X. Shu, "Fabrication and characteristics of eutectic hydrated salts/fumed silica composite as form-stable phase change materials for thermal energy storage," *Solar Energy Materials and Solar Cells*, vol. 238, p. 111584, 2022/05/01/ 2022.
- [32] Y. X. Zhang, A. a. Alizadeh, A. M. Abed, N. Nasajpour-Esfahani, G. F. Smaism, S. K. Hadrawi, H. Zekri, S. Baghaei, S. Esmaeili, and M. X. Wang, "Investigating the effect of size and number of layers of iron nanochannel on the thermal behavior and phase change process of calcium chloride/sodium sulfate hexa-hydrate with molecular dynamics simulation," *Journal of Energy Storage*, vol. 62, p. 106762, 2023/06/01/ 2023.
- [33] N. Kumar, J. Hirsche, T. J. LaClair, K. R. Gluesenkamp, and S. Graham, "Review of stability and thermal conductivity enhancements for salt hydrates," *Journal of Energy Storage*, vol. 24, p. 100794, 2019/08/01/ 2019.
- [34] X. Xiao and D. Wen, "Investigation on thermo-physical properties of molten salt enhanced with nanoparticle and copper foam," in *2018 7th International Conference on Renewable Energy Research and Applications (ICRERA)*, 2018: IEEE, pp. 1445-1449.
- [35] D. N. Nkwetta and F. Haghghat, "Thermal energy storage with phase change material—A state-of-the art review," *Sustainable Cities and Society*, vol. 10, pp. 87-100, 2014/02/01/ 2014.
- [36] A. H. A. Al-Waeli, H. A. Kazem, M. T. Chaichan, and K. Sopian, "Experimental investigation of using nano-PCM/nanofluid on a photovoltaic thermal system (PVT): Technical and economic study," *Thermal Science and Engineering Progress*, vol. 11, pp. 213-230, 2019/06/01/ 2019.
- [37] A. H. A. Al-Waeli, M. T. Chaichan, H. A. Kazem, and K. Sopian, "Comparative study to use nano-(Al₂O₃, CuO, and SiC) with water to enhance photovoltaic thermal PV/T collectors," *Energy Conversion and Management*, vol. 148, pp. 963-973, 2017/09/15/ 2017.
- [38] R. Karwa, "Thermo-hydraulic performance of solar air heater with finned absorber plate forming multiple rectangular air flow passages in parallel under laminar

- flow conditions," *Applied Thermal Engineering*, vol. 221, p. 119673, 2023/02/25/ 2023.
- [39] A. K. Hegde, P. Raghuvir, and K. V. Karanth, "Performance augmentation of solar air heaters: A comprehensive analysis," *Solar Energy*, 2023/02/13/ 2023.
- [40] S. Chand, P. Chand, and H. Kumar Ghritlahre, "Thermal performance enhancement of solar air heater using louvered fins collector," *Solar Energy*, vol. 239, pp. 10-24, 2022/06/01/ 2022.
- [41] A. H. A. Al-Waeli, M. T. Chaichan, K. Sopian, H. A. Kazem, H. B. Mahood, and A. A. Khadom, "Modeling and experimental validation of a PVT system using nanofluid coolant and nano-PCM," *Solar Energy*, vol. 177, pp. 178-191, 2019/01/01/ 2019.
- [42] M. M. Alkilani, K. Sopian, M. Sohif, and M. Alghoul, *Output Air Temperature Prediction in a Solar Air Heater Integrated with Phase Change Material*. 2009.
- [43] V. Dermardiros, Y. Chen, and A. K. Athienitis, "Modelling of an Active PCM Thermal Energy Storage for Control Applications," *Energy Procedia*, vol. 78, pp. 1690-1695, 2015/11/01/ 2015.
- [44] C.-D. Ho, H.-M. Yeh, and T.-C. Chen, "Collector efficiency of upward-type double-pass solar air heaters with fins attached," *International Communications in Heat and Mass Transfer*, vol. 38, no. 1, pp. 49-56, 2011/01/01/ 2011.
- [45] A. Alvarez, O. Cabeza, M. C. Muñiz, and L. M. Varela, "Experimental and numerical investigation of a flat-plate solar collector," *Energy*, vol. 35, no. 9, pp. 3707-3716, 2010/09/01/ 2010.
- [46] A. El-Sebaili, S. Aboul-Enein, M. Ramadan, S. Shalaby, and B. Moharram, "Investigation of thermal performance of double pass-flat and v-corrugated plate solar air heaters," *Energy*, vol. 36, no. 2, pp. 1076-1086, 2011.
- [47] S. Abo-Elfadl, M. S. Yousef, M. F. El-Dosoky, and H. Hassan, "Energy, exergy, and economic analysis of tubular solar air heater with porous material: An experimental study," *Applied Thermal Engineering*, vol. 196, p. 117294, 2021/09/01/ 2021.
- [48] K. S. Ong, "Thermal performance of solar air heaters: Mathematical model and solution procedure," *Solar Energy*, vol. 55, no. 2, pp. 93-109, 1995/08/01/ 1995.
- [49] W. A. B. John A. Duffie, *Solar Engineering of Thermal Processes*, 4th ed. New York: Wiley. (in English), 2013.
- [50] J. Assadeg, A. H. A. Al-Waeli, A. Fudholi, and K. Sopian, "Energetic and exergetic analysis of a new double pass solar air collector with fins and phase change material," *Solar Energy*, vol. 226, pp. 260-271, 2021/09/15/ 2021.
- [51] P. Naphon, "On the performance and entropy generation of the double-pass solar air heater with longitudinal fins," *Renewable Energy*, vol. 30, no. 9, pp. 1345-1357, 2005.
- [52] A. A. Hegazy, "Thermohydraulic performance of air heating solar collectors with variable width, flat absorber plates," *Energy Conversion and Management*, vol. 41, no. 13, pp. 1361-1378, 2000/09/01/ 2000.
- [53] M. Abuşka and S. Şevik, "Energy, exergy, economic and environmental (4E) analyses of flat-plate and V-groove solar air collectors based on aluminium and copper," *Solar Energy*, vol. 158, pp. 259-277, 2017/12/01/ 2017.
- [54] R. Verma, R. Chandra, and H. Garg, "Optimization of solar air heaters of different designs," *Renewable Energy*, vol. 2, no. 4-5, pp. 521-531, 1992.
- [55] A. Fudholi, K. Sopian, M. H. Ruslan, and M. Y. Othman, "Performance and cost benefits analysis of double-pass solar collector with and without fins," *Energy Conversion and Management*, vol. 76, pp. 8-19, 2013/12/01/ 2013.
- [56] A. Bashria, A. Yousef, N. Adam, K. Sopian, A. Zaharim, and M. Alghoul, "Analysis of single and double passes V-grooves solar collector with and without porous media," *Int. J. Energy Environ*, vol. 2, no. 1, pp. 109-114, 2007.
- [57] W. V. Gool, "Energy policy: fairy tales and factualities," in *Innovation and technology—strategies and policies*: Springer, 1997, pp. 93-105.